Mol Cell Proteomics Papers in Press. Published on April 28, 2020 as Manuscript RA120.001981

The DNA sensor cGAS is decorated by acetylation and phosphorylation modifications in the context of immune signaling

Bokai Song, Todd M. Greco, Krystal K. Lum, Caroline Taber, Ileana M. Cristea*

Department of Molecular Biology,
Princeton University, Washington Road, Princeton, NJ 08544

* Corresponding author:
Ileana M. Cristea
210 Lewis Thomas Laboratory
Department of Molecular Biology
Princeton University
Princeton, NJ 08544
Tel: 6092589417
Email: icristea@princeton.edu

Running Title: Post-translational modifications of the cGAS DNA sensor

Abbreviations

cGAS	Cyclic GMP-AMP synthase
STING	Stimulator of interferon genes
TBK1	TANK-binding kinase 1
IRF3	Interferon regulatory factor 3
PQBP1	Polyglutamine-binding protein 1
IFI16	Gamma-interferon-inducible protein 16
TRIM14	Tripartite motif-containing protein 14
XRCC6	X-ray repair cross-complementing protein 6
HEXIM1	Protein HEXIM1
TRIM56	E3 ubiquitin-protein ligase TRIM56
ZCCHC3	Zinc finger CCHC domain-containing protein 3
BECN1	Beclin-1
AKT1	RAC-alpha serine/threonine-protein kinase
CCP5	Cytosolic carboxypeptidase-like protein 5
CCP6	Cytosolic carboxypeptidase 6
NCOA3	Nuclear receptor coactivator 3
NONO	Non-POU domain-containing octamer-binding protein
OASL	2'-5'-oligoadenylate synthase-like protein
LANA	Latency-associated nuclear antigen
HEK293T	Human embryonic kidney 293T cell line
HFF	Human primary foreskin fibroblast cells
THP-1	Human monocytic leukemia cell line
PRM	Parallel reaction monitoring

Abstract

The cyclic GMP-AMP synthase (cGAS) protein is a pattern-recognition receptor of the mammalian innate immune system that is recognized as a main cytosolic sensor of pathogenic or damaged DNA. cGAS DNA binding initiates catalytic production of the second messenger, cyclic GMP-AMP, which activates the STING-TBK1-IRF3 signaling axis to induce cytokine expression. Post-translational modification (PTM) has started to be recognized as a critical component of cGAS regulation, yet the extent of these modifications remains unclear. Here, we report the identification and functional analysis of cGAS phosphorylations and acetylations in several cell types under basal and immune-stimulated conditions. cGAS was enriched by immunoaffinity purification from human primary fibroblasts prior to and after infection with herpes simplex virus type 1 (HSV-1), as well as from immune-stimulated STING-HEK293T cells. Six phosphorylations and eight acetylations were detected, of which eight PTMs were not previously documented. PTMs were validated by parallel reaction monitoring (PRM) mass spectrometry in fibroblasts, HEK293T cells, and THP-1 macrophage-like cells. Primary sequence and structural analysis of cGAS highlighted a subset of PTM sites with elevated surface accessibility and high evolutionary sequence conservation. To assess the functional relevance of each PTM, we generated a series of single-point cGAS mutations. Stable cell lines were constructed to express cGAS with amino acid substitutions that prevented phosphorylation (Ser-to-Ala) and acetylation (Lys-to-Arg) or that mimicked the modification state (Ser-to-Asp and Lys-to-Gln). cGAS-dependent apoptotic and immune signaling activities were then assessed for each mutation. Our results show that acetyl-mimic mutations at Lys384 and Lys414 inhibit the ability of cGAS to induce apoptosis. In contrast, the Lys198 acetyl-mimic mutation increased cGAS-dependent interferon signaling when compared to the unmodified charge-mimic. Moreover, targeted PRM quantification showed that Lys198 acetylation is decreased upon infections with two herpesviruses—HSV-1 and human cytomegalovirus (HCMV), highlighting this residue as a regulatory point during virus infection.

Introduction

The mammalian innate immune system relies on the function of pattern-recognition receptors (PRRs) that are able to recognize pathogen-associated and damage-associated molecular patterns in order to initiate innate immune signaling (1-3). DNA derived either from the genetic material of pathogens or from cellular DNA damage provides such a molecular pattern that can be sensed by PRRs. In recent years, the cyclic GMP-AMP synthase (cGAS) has been characterized as a primary cytosolic DNA sensor during DNA transfection, bacterial infections, DNA virus or retrovirus infection, as well as self-DNA leakage (4-12). During DNA virus infection, cGAS was shown to sense viral DNA upon infection with herpesviruses, including herpes simplex virus 1 (HSV-1) (5, 6), human cytomegalovirus (HCMV) (7, 8), and Kaposi's sarcoma-associated herpesvirus (KSHV) (9), as well as other viruses with DNA as genetic material or DNA intermediates during replication cycle, for example, HIV-1 (10).

The downstream signaling pathway activated by cGAS DNA sensing has been well characterized (Supplementary Figure S1). Upon recognition of DNA, cGAS dimerizes and catalyzes cyclic GMP-AMP (cGAMP) synthesis using GTP and ATP as substrates. cGAMP functions as a second messenger, which binds to and activates STING, an adaptor protein on the endoplasmic reticulum (ER) (4, 13, 14). Activated STING next recruits and activates TANK binding kinase 1 (TBK1), which then phosphorylates IFN regulatory factor-3 (IRF3). The phosphorylated IRF3 dimerizes and translocates into the nucleus to function as a transcription factor and induce the expression of type I interferons and other inflammatory cytokines (15-17). STING also activates IKK, which phosphorylates IκB and thus releases the transcription factor NF-κB into the nucleus, inducing cytokine expressions (18, 19).

As this central cGAS-STING-TBK1-IRF3 immune signaling axis is now well-defined, recent investigation has focused on understanding the regulation of cGAS activity. Several key questions remain to be fully addressed. For example, what drives the recruitment of cGAS to viral DNA during infection? What immune evasion mechanisms have been acquired by viruses via inhibition of cGAS? How do mammalian cells keep cGAS inactive during cellular homeostasis? To this end, a range of protein interactions have been identified that either activate or inhibit cGAS. For example, cGAS associations with PQBP1 (20), IFI16

(21), TRIM14 (22), XRCC6, HEXIM1 (23), TRIM56 (24), ZCCHC3 (25), and NONO (26) were shown to promote immune responses. Other interactions were reported to inhibit cGAS function, including those with BECN1 (27), AKT1 (28), CCP5 and CCP6 (29), NCOA3 (30), caspase-1 (31), and OASL (32, 33). Interactions with viral proteins were also found to underlie the ability of certain viruses to suppress host immune signaling, such as KSHV ORF52 and LANA (9, 34), dengue virus NS2B (35), HSV-1 pUL37 and VP22 (36, 37), and HCMV pUL31 and pUL83 (38, 39).

Another facet of cGAS regulation that has started to emerge is through posttranslational modifications (PTMs). Several cGAS PTMs have been identified, including two phosphorylation sites, two glutamylation sites, one ubiquitination, two SUMOylation sites, and several acetylation sites (24, 28, 29, 40-42). Similar to its protein associations, cGAS PTMs were also shown to have opposing effects on its activity.

Several different types of PTMs were shown to inhibit cGAS functions. For instance, phosphorylation of cGAS by Akt kinase at S305, which is located in the catalytic core of the NTase domain, was shown to suppress its enzymatic activity (28). cGAS was also found to be phosphorylated at Y215 by B-lymphoid tyrosine kinase, which blocks cGAS nuclear translocation upon DNA damage (40). Glutamylation of cGAS was shown to be inhibitory via two different regulatory sites. cGAS monoglutamylation at E302 by tubulin tyrosine ligase-like protein 4 (TTLL4) blocks its synthase activity, and polyglutamylation at E272 by TTLL6 weakens its DNA binding ability (29). Recently, several cGAS acetylation sites (K7, K50, K384, K392, K394, K414) were discovered using mass spectrometry (MS) (42). Among these residues, K384, K394, and K414 acetylations negatively affect cGAS functions in immune signaling. Interestingly, aspirin was shown to directly acetylate K384 and K414, while these modifications could be removed by HDAC3 deacetylase activity (42).

Several PTMs were also found to activate cGAS functions. cGAS monoubiquitination at K335 by the E3 ubiquitin ligase TRIM56 increased cGAS dimerization and DNA binding ability (24). Lastly, murine cGAS was discovered to be SUMOylated by TRIM38 at K217 and K464 (corresponding to K231 and K479 in human cGAS). These two SUMOylation sites inhibit the polyubiquitination of K271 and K464, thus inhibiting the degradation of cGAS. While the murine cGAS SUMOylation at K217 was identified in unstimulated cells, the

K464 SUMOylation was found during HSV-1 infection, and deSUMOylation at this site by Senp2 late in infection caused cGAS degradation (41).

Altogether, these findings paint a picture of cGAS actively and dynamically regulated by PTMs. Given the targeted nature of prior studies, frequently driven by the identification of a cGAS interaction with a specific enzyme, additional analyses can help to expand the knowledge of cGAS PTMs and their existence in different biological contexts, such as under homeostasis and immune activation conditions, and cell types. Here, we investigate cGAS phosphorylations and acetylations in several cell types under basal and immune-stimulated conditions. We start by profiling cGAS PTMs in human primary fibroblasts prior to and during infection with HSV-1, as well as in another system frequently used in the literature for studying cGAS signaling—i.e., STING overexpressing HEK293T cells transfected with DNA 70mers from vaccinia virus (VACV). Altogether, we detected 6 phosphorylation and 8 acetylation sites, of which 5 phosphorylations and 6 acetylations have not been previously documented. The modified sites were analyzed by their sequence conservation and position within the cGAS crystal structure. Validation of PTMs was performed by targeted MS/MS on both tagged and endogenous cGAS using HEK293T cells, fibroblasts and differentiated THP-1 cells. The functional relevance of the PTMs was tested by constructing a series of cGAS mutants that mimic the modified and unmodified PTM states and by measuring the ability of cGAS mutants to induce immune signaling and apoptosis. We find that K384 and K414 acetyl-mimic mutants suppress the induction of cGAS-dependent apoptosis. In contrast, K198Q mutant displayed increased cytokine expression when compared to the K198R mutant, suggesting that K198 acetylation may enhance cGAS function. Additionally, quantification of K198 acetylation by targeted MS/MS demonstrated decreased acetylation levels upon infection with HSV-1 and HCMV when compared to uninfected cells. Taken together, these results point to K198 acetylation as a regulatory cGAS modification during viral infection.

Experimental Procedures

Antibodies & Reagents

Below are the primary antibodies used in Western blotting: cGAS (HPA031700; Sigma), GFP (11814460001; Roche), tubulin (T6199; Sigma-Aldrich), pIRF3 (ab76493; Abcam), PARP (9542L; Cell Signaling Technology). Goat anti-Rabbit and Goat anti-Mouse IgG (H+L) Secondary Antibody, Alexa Fluor® 680 conjugate (A-21058 and A-21109; Thermo Fisher Scientific), as well as IRDye 800CW Goat anti-Rabbit and Goat anti-Mouse IgG (H+L) (92632211 and 92632210; LI-COR) were used as Western blotting secondary antibodies. For immunoaffinity purification, anti-GFP antibody (in-house) and cGAS antibody (ARG54961; Arigo) was used.

Primers

CRISPR-cGAS sgRNA target sequence: AGACTCGGTGGGATCCATCG

qPCR-β-Actin forward: TCCTCCTGAGCGCAAGTACTC

qPCR-β-Actin reverse: CGGACTCGTCATACTCCTGCT

qPCR-IFN-β forward: GCATTACCTGAAGGCCAAGG

qPCR-IFN-β reverse: AAGCAATTGTCCAGTCCCAGA

qPCR-ISG54 forward: ACGGTATGCTTGGAACGATTG

qPCR-ISG54 reverse: AACCCAGAGTGTGGCTGATG

(Integrated DNA Technologies)

Plasmid & Cell Line Construction

EGFP-hcGAS was generated by overlap-extension PCR and ligated into pcDNA3.1 vector between *KpnI* and *XhoI* sites. In order to be expressed in the cell line, EGFP-hcGAS sequences were subcloned into LentiORF pLVX-TetOne-Puro vector, which was purchased from Open Biosystems. pcDNA3.1-EGFP-hcGAS plasmids with point mutations were generated by site-directed mutagenesis.

Construction of HEK293T-STING was described in (43). To construct EGFP,

EGFP-hcGAS and hcGAS-EGFP HFFs, the WT HFFs were transduced with lentivirus generated from pLVX-TetOne-Puro-EGFP, pLVX-TetOne-Puro-EGFP-hcGAS or plasmid for three days and selected in 2 μg/ml puromycin for a week. To construct HEK293T-STING-EGFP and HEK293T-STING-EGFP-hcGAS cells, the HEK293T-STING cells were transduced with respective lentiviruses, and the cells were selected through fluorescence-activated flow cytometry (S3 Cell Sorter, BioRad). The expression of EGFP and EGFP-hcGAS can be induced by doxycycline (1 μg/ml for EGFP, 2 ug/ml for EGFP-hcGAS).

Mutant EGFP-cGAS HFF cell lines were constructed by transducing pLVX-TetOne-Puro-EGFP-cGASmutant plasmid into cGAS KO HFFs. The CRIPSR knockout was done by transfection of Cas9 and gRNA, using Lipofectamine™ CRISPRMAX™ Cas9 Transfection Reagent (Thermofisher).

Tissue culture and Viruses

Primary human foreskin fibroblasts (HFFs) and HEK293T cells were cultured in Dulbecco's modified Eagle medium with 10% fetal bovine serum, penicillin (100 U/mL) and streptomycin (100 mg/mL) and maintained at 37°C in a 5% CO_2 environment. The HFFs were provided generously by Dr. Hillary Coller of University of California Los Angeles, USA. THP-1 cells (ATCC) were cultured in RPMI-1640 medium with 10% fetal bovine serum, penicillin (100 U/mL) and streptomycin (100 mg/mL) in cell culture flasks. THP-1 cells were differentiated in culture media with 1 μg/mL phorbol 12-myristate 13-acetate (PMA; Sigma-Aldrich) for 48 h.

Lentiviruses were generated in HEK293T cells. The lentiviral transfer vector was co-transfected with lentiviral packaging vectors psPAX2 and VSV-G into HEK293T cells, with a ratio of 1:1.5:1. Lentiviruses were collected at 40, 56, and 72 h post-transfection in 30% FBS DMEM, and filtered using a 0.45 μm membrane. The lentiviruses were kept at -80°C until use.

WT HSV-1 was generated using the bacterial artificial chromosome (BAC) with the full HSV-1 (17+ strain) genome carried by *E. coli* strain GS1783, which was a gift from Dr. Beate Sodeik of Hannover Medical School (Hannover, Germany). The pBAC-HSV-1 was

electroporated into Vero cells in order to generate P_0 WT HSV-1. HCMV (Ad169 strain) was a gift from Dr. Thomas Shenk of Princeton University and were produced in HFFs. To produce progeny viruses, the cells were infected with virus at MOI of 0.001, and then the cells and media were collected when 100% cytopathic effect was observed. The media was centrifuged at 20,000 rpm (Beckman SW28) for 2 h at 4°C, and the viruses were resuspended in MNT buffer (200 mM MES, 30mM Tris-HCl, 100 mM NaCl, pH 7.4). The infected cells were resuspended in MNT buffer and sonicated to release cell-associated viruses. The cell-free and cell-associated viruses were combined and kept at -80°C until use. Viral titers were acquired by plaque assays (HSV-1), and by TCID50 (HCMV).

Plasmid and VacV 70mer Transfections

For packaging lentiviruses in HEK293T cells, and VacV 70mer transfection, X-tremeGENE HP transfection reagent (Roche) was used according to the manufacturer's protocol. For other transient transfection experiments, Lipofectamine 2000 (Life Technologies) was used according to manufacturer's protocol. The ratio of transfection reagent to DNA was 2 µl: 1 µg.

RNA isolation and qRT-PCR

Cellular RNA was isolated using the RNeasy Mini kit (Qiagen). DNaseI (Invitrogen) was used to digest DNA contaminants. The reverse transcription step was done with the RETROscript Reverse Transcription kit (Life Technologies). The quantitative PCR step was done on the ViiA 7 real-time PCR system (Applied Biosystems), using SYBR green PCR master mix (Life Technologies) and gene specific primers (IDT). The delta delta Ct method was applied to quantify the relative mRNAs abundance of each specific gene, using β-actin as the internal reference.

Cell lysis and immunoaffinity purification

Cells were washed in PBS, and then scraped off the plates using cell lifters. After a 5 min centrifugation at 250 x g, the cells were lysed in lysis buffer (20 mM HEPES, pH 7.4, 10 mM KCl, 2 mM $MgCl_2$, 1 mM DTT, 200 mM NaCl, 1% (v/v) Triton X-100, 0.11 M KOAc, 1%

(v/v) Tween-20, 0.5% (v/v) NP-40, 1/100 protease inhibitor cocktail (PIC, Sigma), 1/100 phosphatase inhibitor cocktail (PhIC, Sigma), and 100U/ml benzonase) for 30 min on ice, with vortexing every 5 min. The lysate was subjected to polytron homogenization and centrifuged at 8000 x g for 10 min to pellet insoluble material. The supernatant was recovered and processed by immunoaffinity purification. Antibody-conjugated magnetic beads were prepared as previously described (43). Immunoaffinity purification was performed using 1 mg of Dynabeads Magnetic Beads (Thermo Scientific) conjugated with either α-GFP or α-cGAS antibody (5µg antibody/mg magnetic beads). Conjugated beads were incubated with supernatants for 1 h at 4 °C. Beads were washed six times with lysis buffer and once with PBS, then incubated with elution buffer (1x Laemmli sample buffer) for 10 min at 70 °C.

SDS-PAGE and western blotting

Cells were lysed in 1x Laemmli sample buffer (62.5 mM Tris-HCL, pH 6.8, 2% SDS (w/v), 10% glycerol (v/v), 0.02% bromophenol blue (w/v), 100 mM DTT) and boiled at 95°C for 10 min. Samples were resolved by SDS-PAGE using Tris-Glycine gel (10%). The proteins were transferred to PVDF membranes by wet transfer method, blocked with 5% (w/v) milk in PBS, and incubated with primary and secondary antibodies. Protein bands were detected and quantified by immunofluorescence using a LI-COR Odyssey imaging system (LI-COR Biotechnology).

Experimental Design and Statistical Rationale

Data-dependent LC-MS/MS experiments were performed in 4 independent biological replicates per condition (see Fig. 1D). This was selected as appropriate for building spectral libraries of cGAS PTMs while accounting for experimental variation and stochastic nature of MS/MS sampling. Parallel reaction monitoring experiments were performed to target PTM candidates for validation in 3 independent biological replicates of HEK293T and human fibroblasts (HFF) and 2 biological replicates of THP-1. Unpaired t-tests were performed in Excel or GraphPad Prism to test for statistical significance.

In-gel digestion and nanoliquid chromatography-tandem mass spectrometry analysis

The IP elution samples were processed by SDS-PAGE and in-gel digestion, as previously described (43). Briefly, proteins were reduced by 25 mM tris(2-carboxyethyl)phosphine and alkylated by 50 mM chloroacetamide, and then separated on a NuPAGE 4-12% BisTris gel (Invitrogen). Protein bands were visualized by Coomassie blue. The region of the gel corresponding to either GFP-cGAS or untagged cGAS were excised and the in-gel digestion was performed using trypsin (Promega). Peptides were desalted using SDB-RPS stage tips (44), concentrated to near dryness by vacuum centrifugation, and resuspended in 1% formic acid (4 µl).

Desalted peptides (2 µl) were analyzed by data-dependent LC-MS/MS using a Top 15 acquisition strategy on an LTQ Orbitrap Velos-ETD (Velos) (43, 45, 46) or Q Exactive HF Hybrid Quadrupole-Orbitrap (QE) mass spectrometer (47, 48) equipped with an EASY-Spray or Thermoflex ion source, respectively, and interfaced with Dionex Ultimate 3000 nanoRSLC HPLCs (Thermo Scientific). Briefly, peptides were separated by direct injection over an EASY-Spray PepMap C18 column (2 µm; 25 cm x 75 µm, Velos) or self-packed Reprosil C18-AQ column (1.9 µm; 20 cm x 75 µm, QE) for 90 min (Velos) or 60 min (QE) at 250 nl min^{-1} with a reverse phase linear ACN gradient from 4 to 40% (Velos) or 5 to 32% (QE) solvent B (B: 97% ACN/0.1% formic acid/2.9% water, A: 0.1% formic/99.9% water). One cycle of data-dependent acquisition consisted of a precursor scan in the orbitrap at resolution of 30,000 (Velos) or 120,000 (QE), followed by MS/MS on the top 15 precursors using collision-induced dissociation (CID, Velos) or higher-energy collisional dissociation (HCD, QE). Fragment ions were detected in the ion trap (Velos) or orbitrap (QE). See Figure S2 for detailed instrument-specific parameters.

Data Processing and PTM identification

Raw instrument files were processed through either Proteome Discoverer 1.4 (Thermo Scientific)/Scaffold 4.6.2 (Proteome Software, Portland, OR), or Proteome Discoverer 2.2 (Thermo Scientific), using default parameters with modifications, as noted. The processing of raw data files consisted of 1) extraction of MS/MS spectra and assignment of the monoisotopic precursor peak, 2) Peptide Spectrum Match (PSM) assignment using SEQUEST HT (v1.3 or 1.17) against a database of human and herpesvirus protein sequences

appended with common contaminants (UniProt Reference Proteome, 2015-09; 70,155 sequences or UniProt Swiss-Prot, 2016-04; 22, 213 sequences), 3) validation of primary search scores using Scaffold or Percolator (v3.0), and 4) scoring of phosphosites by phosphoRS (v3.1) or ptmRS (v2.2) (49). For ion trap-CID spectra, SEQUEST was configured as follows: precursor and fragment tolerances, 10 ppm and 0.5 Da; full trypsin specificity with maximum of 2 missed cleavages; static modification of Cys carbamidomethyl; variable modification of STY phosphorylation. For matching of HCD spectra (Q Exactive HF), SEQUEST was configured as follows: precursor and fragment tolerances, 4 ppm and 0.02 Da; full trypsin specificity with maximum of 3 missed cleavages; static modification of carbamidomethyl (C); variable modifications of deamidation (N), acetylation (K), phosphorylation (STY), and protein terminus MetLoss+Acetyl. Scaffold and X! Tandem (50) were used for post-processing of SEQUEST PSMs from Proteome Discoverer 1.4. X! Tandem re-search was performed in Scaffold with the subset database enabled. SEQUEST and X! Tandem PSMs were combined and assigned peptide probabilities using the Scaffold LFDR algorithm (51). Percolator (52) was used with default settings for post-processing of SEQUEST PSMs from Proteome Discoverer 2.2. For all workflows, PSM were filtered to a peptide false discovery rate of 1% using q-values that were calculated based on PSM score distributions for reverse database searches. Manual inspection of MS/MS spectra assigned to post-translationally modified cGAS peptides was performed using Scaffold or consensus workflows (PD 2.2). Only PTM sites with site localizations scores > 0.75, corresponding to an estimated false localization rate of < 1% (49), were considered. Overall cGAS sequence coverage was obtained by combining data-dependent experiments into a Skyline spectral library, then plotted using Protter (http://wlab.ethz.ch/protter/) (53).

Development and Analytical Validation Targeted MS Assays/Measurements

PRM methods were developed according to as Tier 3 level analyses. PRM method design and data analysis was performed using Skyline (54) (ver. 19.1). Initial PRM methods were created with wide retention time scheduling windows (15 min) containing 14 PTM peptides and two unmodified peptides from spectral libraries assembled from data-dependent search results. Using these initial PRM methods, cGAS peptides from pooled samples (2 µl) were analyzed

by LC-MS/MS on a Dionex Ultimate 3000 nanoRSLC HPLC connected online to a Q Exactive HF Hybrid Quadrupole-Orbitrap (QE) mass spectrometer equipped with an EASY-Spray ion source (Thermo Scientific). Peptides were separated by direct injection over an EASY-Spray PepMap C18 column (2 µm; 25 cm x 75 µm, Velos) for 60 min at 250 nl min^{-1} with a reverse phase linear ACN gradient from 3 to 30% solvent B (B: 97% ACN/0.1% formic acid/2.9% water, A: 0.1% formic/99.9% water). The mass spectrometer was configured for parallel reaction monitoring (PRM) acquisition (see Fig. S2). The detection of modified peptides was manually evaluated. Refined scheduled PRM methods were generated without MS1 precursors scans, and with larger maximum injection times and narrower retention time windows, allowing for a reduction in the number of concurrent precursors to ≤ 3. Refined PRM methods were applied to biological replicates (N = 3) of uninfected HEK293T, HFF, and THP-1 cells. Validation of PTMs in Skyline was performed by manual verification of peak picking. A candidate PTM was considered validated if it was detected ≥ 2 independent samples with ≥ 4 co-eluting fragment ions and received a dotp score > 0.70 (see Fig. S3 for targeted peptides and their fragment ions). For targeted quantification of acetyl-lysine 198 in uninfected and herpesvirus-infected HFF cells, co-elution of fragment ion chromatogram, absence of interferences, and integration boundaries were manually validated. The top three peak areas for the validated fragment ion chromatograms were summed, normalized by total cGAS levels using the unmodified peptide IQLEEYSNTR, and expressed relative to the average of the uninfected samples (mean ± SEM, N=3).

Results

cGAS contains multiple acetylation and phosphorylation sites

PTMs are dynamically regulated by different external stimuli, and this regulation often occurs in a cell type dependent manner. To improve the likelihood of identifying cGAS PTM sites that have potential biological relevance, our initial analysis employed non-targeted, data-dependent mass spectrometry performed in two cell types that express GFP-tagged cGAS and under conditions that stimulate cGAS activity. First, to verify that the N-terminal tagged cGAS retains its immune stimulatory function, we co-transfected GFP-cGAS and STING into HEK293T cells. These cells do not endogenously express cGAS or STING and

were shown to provide a platform for reconstituting and testing the cGAS-signaling pathway (5, 55). We found that GFP-cGAS stimulated anti-viral cytokine induction, demonstrated by measuring interferon-β (*ifn-β*) and interferon stimulated gene 54 (*isg54*), and by blotting against phosphorylated IRF3 (Fig. 1 A-C). Next, we generated doxycycline-inducible cell systems expressing GFP-cGAS using lentiviral transduction in human primary fibroblasts (HFFs), as well as in STING-expressing HEK293T cells. In agreement with previous reports (21, 40, 56, 57), GFP-cGAS localized to both the cytoplasm and the nucleus, with a more prominent cytoplasmic localization (Fig. 1D).

As PTMs are often present at sub-stoichiometric ratios, the assembly of proteome-scale PTM databases has benefited from the use of affinity enrichment approaches paired with tandem MS analysis (58, 59). These approaches have supported clinical investigation of PTMs, such as phosphorylations involved in immune responses (60), and more generally, PTMs associated with disease phenotypes (61). In the current study, we leveraged the concept of enrichment by isolating the cGAS protein from cells using immunoaffinity purification coupled to mass spectrometry (IP-MS) (Fig. 1C), which can offer PTM enrichment in a modification-independent fashion (as in (46, 62, 63)). IP-MS analysis of GFP-cGAS was performed from fibroblasts that were either uninfected (mock) or HSV-1 infected at 6 hours post infection (hpi), a time point at which cGAS-mediated cytokine induction has been reported (5). Additionally, GFP-cGAS IP-MS analyses were performed from HEK293T cells 6 hours post transfection (hpt) with VacV70mer DNA, which has been shown to induce cytokine induction through the cGAS-STING pathway (64).

Analysis of the immunoisolated GFP-cGAS using nLC-MS/MS (on an LTQ Orbitrap Velos or Q Exactive HF mass spectrometer) afforded an overall sequence coverage of 82% (Fig. 1F and Fig. S4) and led to the identification of 14 cGAS PTMs (PTM site localization scores > 0.99), which included six phosphorylation and eight acetylation sites (Fig. 1F and 1G, Fig. S5). Notably, pS305 was identified, which was previously reported to be phosphorylated by Akt kinase, dampening cGAS enzymatic activity (28). Among previously reported acetylation sites, acetylation of K50 and K384 were present in the current analysis. To our knowledge, the remaining 11 modified sites have not been previously identified or characterized.

Several conserved modified sites show proximity to DNA and/or have high solvent accessibility

To gain insight into which modifications may contribute to cGAS functions, the locations of the modified residues within the human and mouse cGAS crystal structures (65, 66) were evaluated, as well as their sequence conservation among various species. As previously reported, in the human cGAS structure, S305 is located in the catalytic core and its phosphorylation inhibits cGAMP synthesis (28). K384 is located in close proximity to the bound DNA, and its positive charge has been shown to contribute via hydrogen bonding to the DNA binding ability of cGAS. Hence, the K384 acetylation would partially neutralize this charge, consistent with the finding that this modification inhibits DNA binding (42). In addition to these two previously characterized sites, our investigation showed that S221 is located within the NTase core, while K198 and K355 are close to the bound DNA (Fig. 2A and Fig. S6).

Using the human protein structure, the accessible surface areas (ASA) for the identified PTM sites were determined using the online tool PDBePISA (67). ASA values could be calculated for nine of the fourteen PTM sites. Overall, the average ASA for these PTM sites was greater than the average of all cGAS residues (Fig. 3B). Several modified residues, such as at K198 and K432, had relatively high ASA values, while S305, which is buried in the catalytic core, had a low ASA value. While the functional relevance of PTM sites is not exclusively linked to their surface accessibility, this analysis suggests that PTM sites with higher ASA values may be positioned to participate in cGAS protein interaction interfaces.

Investigation of the phylogenetic sequence conservation of candidate cGAS PTM sites showed that, in addition to the known S305 and K384 sites, S221 and K285 are also well conserved among different species (Fig. 3). Additionally, the K198 site shows an intriguing pattern, i.e., being switched between K and Q amino acids among mammalian species, which suggests that acetylation at this residue position may have an evolutionary importance. Given the potential functional implications of our candidate PTMs within the sequence and structural features of cGAS, we wanted to further validate the presence of these candidate PTMs and analyze their functional relevance.

Validation of PTMs on GFP-cGAS and endogenous cGAS

While discovery proteomics approaches allowed for greater breadth of PTM detection, not all cGAS PTM sites were detected across all samples and replicates. Historically, the issue of stochastic sampling by unbiased approaches can be remedied by high resolution, data-independent and targeted mass spectrometry approaches that validate and quantify phosphorylation and acetylation with improved sensitivity and reproducibility (68-70). Here, to determine the PTMs that are reproducibly present, we performed targeted mass spectrometry of cGAS PTMs using parallel reaction monitoring (PRM) on a Q Exactive HF (Fig. 4A). To build the targeted PRM method, spectral libraries were assembled from data-dependent analyses. The best responding tryptic peptides (by MS1 intensity and fragmentation pattern) for the 14 cGAS PTM sites were selected, along with two unmodified cGAS peptides as positive controls (Fig. S3). PRM experiments were first performed in HEK293T and HFF cells that expressed GFP-cGAS to confirm the presence and site localization of the modifications following cGAS immunoisolation. cGAS PTMs were considered validated if they were detected in at least two biological replicates, and with ≥ 4 co-eluting fragment extracted ion chromatograms that matched the library spectrum (dotp score ≥ 0.7). Overall, 11 PTM sites, corresponding to five phosphorylation and six acetylation sites, were confirmed in HEK293T cells (Fig. 4B). Of note, the general trend of lower dotp scores for phosphopeptides was likely due to the differences in fragment ion intensities between the PRM-acquired MS/MS spectra (HCD) versus the MS/MS spectra in the library (ion trap CID). In primary fibroblasts (HFFs), seven PTM sites were validated—three phosphorylations and four acetylations (Fig. 4C). The ability to validate more modifications in 293T cells compared to HFFs is likely in part due to the higher GFP-cGAS expression level. Interestingly, despite the possibility for positional isomers for several of the phosphopeptides, the PRM analysis did not detect site determining fragment ions to support these alternative modification sites. This observation is consistent with the high PTM site localization scores for cGAS modified peptides (Fig. 1G).

We next aimed to validate cGAS PTMs on endogenous cGAS. We focused on the immune-relevant THP-1 monocytes differentiated into macrophages-like cells, in which

cGAS has been shown to be expressed and active (71). The isolation of endogenous cGAS proved challenging, and several commercially available anti-cGAS antibodies were tested. While the isolation of endogenous cGAS was less effective than from the GFP-tagged cells, our analysis confirmed four modified sites—phosphorylation of S116 and S305 and acetylation of K198 and K355 (Fig. 4D).

Although it is difficult to compare across cell types due to different cGAS levels and capture antibodies, the most consistently detected phosphorylations across all cell types were S305 and S116, while K198 was the most reproducible acetylation site. Two of these consistent modifications, pS116 and Kac198 (Fig. 4E and Fig. S7), have not been previously documented. Broadly, our results show that cGAS, either endogenously or upon expression, can be modified on at least 11 residues. Having confirmed these cGAS PTMs, we next investigated their functional relevance.

Phosphorylation of S305 and acetylation of K384 and K414 inhibit cGAS-dependent apoptosis

Upon binding to dsDNA, cGAS has previously been shown to induce downstream immune signaling and apoptosis (4, 5, 43). To characterize the potential role of cGAS PTMs in these downstream signals, we generated a set of GFP-cGAS PTM mutants for each of the modified residues (Fig. 5A). Specifically, for each site that we identified as phosphorylated, we generated S-to-A and S-to-D cGAS mutants to represent the unphosphorylated and phosphorylated state, respectively. Additionally, for each acetylated residue identified, we constructed K-to-Q and K-to-R mutants to mimic the acetylated and the unmodified positively charged state, respectively.

The impact of these substitutions on the ability of cGAS to induce apoptosis was assessed by measurement of polyADP-ribose polymerase 1 (PARP1) cleavage in STING-expressing HEK293T cells co-transfected with mutant or WT GFP-cGAS, or GFP control. As HEK293T cells do not express endogenous cGAS, these cells allowed the assessment of the specific impact of the mutations on cGAS functions. The expression of GFP-cGAS and associated PTM mutants did not cause any overt changes in cell and nuclear morphology (Fig. S8), while the levels of cGAS constructs were similar (Fig. 5B-C). From

the perspective of apoptosis induction, PARP1 cleavage in the S305D mutant was lower compared to WT, indicating that the S305 phosphorylation can have an inhibitory effect on cGAS-mediated apoptosis. Among the acetylation sites that we detected, the K384Q mutant led to inhibited PARP cleavage. In a prior study, K384, K394, and K414 acetylations inhibited cGAS-dependent cytokine production (42). Given this shared functionality, we predicted that the K394Q and K414Q mutants might inhibit cGAS-dependent apoptosis. Indeed, we found that the K414Q and K414R mutants resulted in inhibition of PARP cleavage, while the K394Q mutant did not impact this function. Our observation that both (Q & R) mutants of K414 resulted in the same effect on apoptosis may not be surprising as these mutants have also shown a concordance in their inhibition of cGAS-dependent cytokine production (42). Overall, the present experiments provide the first evidence that cGAS post-translational modification may participate in cGAS-mediated apoptosis. Therefore, these PTM sites could be of particular relevance for understanding the molecular mechanisms of virus-host defense.

K198 acetylation results in increased cGAS-mediated cytokine induction

We next investigated the impact of cGAS mutations on its ability to induce cytokine expression, by measuring the mRNA levels of IFN-β and ISG54 in STING-expressing HEK293T cells co-transfected with WT or mutant GFP-cGAS, or GFP control (Fig. 6). The S305A/D and K384Q/R mutants were used as positive controls, given their described roles in cGAS immune signaling (28, 42). As expected, we observed that the S305D and K384Q mutants, which mimicked the phosphorylated and acetylated residues, inhibited the induction of antiviral cytokines. Mutation of the other identified phosphorylation sites did not show significant changes in cytokine induction. However, the K198Q mutation resulted in increased cytokine expression when compared to the K198R mutation. This result suggested that K198 acetylation may enhance cGAS function, leading to higher expression levels of anti-viral cytokines (Fig. 6).

K198 acetylation modulates cGAS signaling and is decreased during infection with both HSV-1 and HCMV

cGAS has been shown to promote immune signaling following infection with either HSV-1 or HCMV (4, 5, 7). Given our finding that K198 mutants differentially impacted cytokine expression, we aimed to further characterize this site in the context of viral infection. We first generated primary human fibroblasts (HFF) that lack cGAS through CRISPR-mediated knockout (Fig 7A). Then, in this background, we generated cells stably expressing K198Q and K198R GFP-cGAS. This allowed us to study cGAS-dependent signaling upon HSV-1 infection, using the levels of phosphorylated IRF3 as a proxy for immune signaling. We employed K384Q, K414Q and K414R mutants, which were previously reported to modulate cGAS function (42), as controls (Fig. 7B). The expression of the K198Q mutant led to higher levels of phosphorylated IRF3 levels than the K198R mutant (Fig. 7B), which was consistent with our results on IFN-β expression (Fig. 6). Together, these data suggest a role for K198 acetylation in cGAS-dependent immune signaling.

PTM-dependent regulation of protein activity and cell signaling often involves changes in modification stoichiometry. Therefore, we investigated whether the level of K198 acetylation is regulated during viral infection. We performed relative quantification of K198 acetylation in GFP-cGAS-expressing uninfected fibroblasts and cells infected with either HSV-1 or HCMV at 6 hpi using targeted MS/MS (see Fig. 4). Following GFP-cGAS IP, the Kac198 peptide was measured by PRM, normalized by total cGAS levels, and then expressed relative to the average of the uninfected samples (see Experimental Procedures). K198 acetylation levels showed significant decreases following both HSV-1 and HCMV infections (Fig. 7C). This finding is intriguing given the surface accessibility of this site (Fig. 2) and its functional relevance in cGAS immune signaling (Fig. 6 & 7), highlighting K198 as a regulatory point for modulating cGAS functions during pathogen infections.

Discussion

cGAS has been characterized as a pivotal cytoplasmic DNA sensor against pathogen infections and self-DNA leakage (4-12). In addition, cGAS is also reported to play crucial roles in senescence, autophagy (72), and cancer (73). For example, cGAS links DNA damage and cellular senescence and is essential for senescence phenotypes (56). However, in cancer biology, cGAS is a double-edged sword, as it can contribute to either anti-tumor immunity or

inflammation-driven carcinogenesis and metastasis (74). Overall, given the exquisite control needed to engage in physiological immune signaling, the underlying molecular mechanisms that control cGAS-dependent signaling are of broad interest. These explorations provide mechanistic explanations for how IFNs and danger signals are dynamically tuned by the cell to both regulate homeostasis and clear pathogen infections.

Profiling cGAS post-translational modifications

Towards this goal, we wanted to broaden the scope of knowledge for the regulation of cGAS-dependent activities by post-translational modification. To enable sensitive PTM detection that was not biased to a particular modification, we employed immunoaffinity purification of cGAS and "bottom-up" DDA sequencing using CID and HCD fragmentation techniques. When targeting multiple modifications on a single protein target, intact protein-based immunoaffinity enrichment techniques are more efficient and often find PTMs not identified by proteome scale affinity enrichment approaches. This is arguably best exemplified by the mass spectrometric characterization of histones (75), but has also been observed for other proteins (63, 70). In this study of cGAS PTMS, we initially detected 14 PTMs on cGAS. These PTMs did not include several sites characterized by prior studies, such as pY215, Kac394, and Kac414 (40, 42). This could be due to biological and technical differences, including cell type specificity, epitope tagging, and sample preparation.

Of the 14 putative PTMs detected in this study, we reproducibly validated 11 sites by parallel reaction monitoring. Interestingly, the breakdown of sites by modification type was roughly equivalent, five phosphorylation and six acetylation sites. Given the majority of serine and threonine phosphorylations typically have greater stoichiometry (1-30%) compared to lysine acetylation (< 1%) (76-78), the nearly equivalent detection is intriguing. The three PTM sites that were detected by the DDA analyses, but not validated by PRM may be due to their low abundance, either in absolute terms or in unstimulated cells. Although we did not detect other "common" lysine modifications, such as lysine succinylation, malonylation, or lysine/arginine mono-, di-, or tri-methylation, the global protein PTM landscape is vast and it is likely that cGAS is modified at residues our DDA analyses did not detect. For example, the GFP tag may have induced cGAS conformational changes that

altered its modification status compared to the untagged protein. Our data from endogenous cGAS isolated from THP-1 argues against this possibility, but the differences in cGAS abundance between the cell lines prevent a direct comparison. Overall, our results show that cGAS is highly decorated by PTMs, identifying eight previously unreported modification sites, while also providing the basis for future experiments that target additional PTMs.

Interferon-independent roles for cGAS PTMs

The STING-IRF3 signaling axis has been shown to activate the mitochondrial apoptotic pathway independent of transcription induction, i.e. interferon-β production, during RNA virus (79) and human T cell leukemia virus 1 infection (80), and ER stress (81). cGAS has also been shown to induce apoptosis by a non-transcriptional mechanism during HSV-1 infection (32) or mitotic cell death (82). Our study provides a previously unrecognized aspect of cGAS regulation, showing that cGAS PTMs can regulate the induction of apoptosis. Our findings suggest that several PTMs modulate cGAS-mediated apoptosis and cytokine expression either differentially (e.g., Kac198, Kac394) or concordantly (e.g., pS305, Kac384, Kac414). By employing stable cell lines expressing cGAS PTM blocking and mimicking mutants for 16 unique PTM sites (identified from this study and previous work (28, 42), we determined that pS305, Kac384, and Kac414, are likely modulatory PTMs during cGAS-dependent apoptosis induction. For all sites, PTM mimicking mutants (S-to-D and K-to-Q) resulted in inhibition of PARP cleavage. For many viruses, induction of apoptosis is often delayed until the virus can sufficiently replicate and release progeny virus, which facilitates the propagation of infection (83). Based on our data, it is tempting to speculate that DNA viruses have evolved mechanisms to delay apoptosis in part by modulating the modification state of cGAS at S305, K384, and K414.

The structure-function relationship of cGAS K198 acetylation

Our site-directed mutational analysis of K198 to mimic the acetylated (Q) or non-acetylated (R) lysine resulted in opposing magnitudes of *ifn-β* mRNA induction (see Fig. 6). Our observation that the WT condition produces an intermediate *ifn-β* response, compared to the K to Q and K to R mutants, is consistent with the mixture of unmodified and acetylated

K198 we find in unstimulated cells. These results are highly suggestive that K198 acetylation could modulate signaling during immune activation. Indeed, when cells were challenged with HSV-1 infection, the K198 site mutants again showed opposing responses, specifically in IRF-3 phosphorylation, a downstream effector of cGAS signaling. Finally, both HSV-1 and HCMV infection alone downregulate K198 acetylation. Taking these results together, it is possible that the stoichiometry of Kac198 can calibrate the magnitude of cGAS activation to increase downstream interferon signaling. Interestingly, K198Q does not appear to impact cGAS-dependent apoptosis, and thus it is possible that K198 acetylation provides a mechanism for which cGAS-dependent cytokine induction is distinct from cGAS-dependent apoptosis induction. Given these findings, it is tempting to speculate that K198 acetylation would promote antiviral cytokine expression in the context of viral infection, thereby limiting efficient viral replication and spread. The observed infection-induced decreases in cGAS K198 acetylation levels may reflect a viral innate immune evasion strategy. For example, if acetylation levels are different between infection with WT virus versus a mutant virus strain that lacks the ability to antagonize cGAS and suppress cytokine induction (e.g., HSV-1 UL37C819S (36) or HCMV v65Stop (39)), then the innate viral mechanisms that modulate cGAS acetylation levels would warrant future investigation.

Yet, at present, the molecular mechanism(s) by which K198 acetylation increases cGAS function are unclear. From a structural perspective, previous research of the cGAS-DNA binding structures (65) suggested that certain lysine acetylations would inhibit cGAS binding with negatively charged DNA through neutralizing the positively charged lysine and thus would inhibit cGAS signaling. Indeed, the previously identified acetylation at K384 is located in close apposition to bound DNA and was found to impact its DNA binding ability and inhibit cGAS function (42, 65). Although K198 is located close to the bound DNA on the cGAS structure, based on our hypothesis that increased K198 acetylation potentiates signaling, it is unlikely that acetylation of this residue impacts cGAS DNA binding. It is possible that K198 acetylation affects cGAS function by inducing conformational change. This residue is localized at the C-terminus of an alpha-helix and may alter the orientations of the residues nearby. It is also possible that K198 acetylation, owing to its relatively high surface accessibility, may influence cGAS protein-protein interactions that are modulators of

its enzymatic activity.

Taking a broader perspective on the function of K198 acetylation, we observed from the sequence conservation analysis of cGAS PTM residues that the K198 position was exclusively K or Q among all mammals and fish. The Q alternate at the 198 position is intriguing as a biochemical mimic of the charge neutralization effect imparted by acetylation on the ε-amino group of lysine. Therefore, the prevalence of Q at this position might indicate a selective benefit to fitness, perhaps by offering a greater cGAS signaling threshold. One could also argue that the presence of K confers a selective advantage, which would be through a different mechanism and thus would not exclude the Q advantage. Specifically, K may provide state-dependent acetylation regulation. It is notable that K is exclusively conserved among higher primates. Given our results with herpesviruses, it is tempting to speculate that the co-evolution of hosts and viruses has played an important role in driving the development of new mechanisms for both innate immune stimulation and evasion by pathogens. Higher primates may take advantage of the K residue to restrict cGAS function under quiescence, while viruses that infect these species may have acquired the ability to decrease the acetylation level, thus dampening cGAS antiviral functions.

Overall, our identification of previously unreported cGAS PTMs allowed us to systematically screen these positions for their roles in specific cGAS functions. The identification of functionally selective PTMs provides new insights into cGAS regulation under active immune signaling. As cGAS is also shown to play important roles in senescence, autophagy, autoinflammatory diseases, and cancer (72, 73), this study provides additional PTM sites that may influence cGAS functions in these other pathological states. Among these roles, the distinct activities of the explored PTMs have meaningful implications for explaining the evolutionary history of cGAS functions, from those suggested to be primordial (e.g., autophagy) to those suggested to have developed adaptively (e.g., interferon stimulation).

Acknowledgements

We thank Gary Laevsky (Princeton University microscopy facility) for technical support. Funding was provided by NIH NIGMS (GM114141) and by the Edward Mallinckrodt

Foundation to I.M.C., China Scholarship Council (CSC) scholarship (201506210052) to B.S., and NIH Ruth L. Kirschstein F31 fellowship (GM120936) to K.K.L, and the NIH training grant from NIGMS (T32GM007388).

Data Availability

Data-dependent mass spectrometry data have been deposited to the ProteomeXchange Consortium via the PRIDE (84) partner repository with the dataset identifier PXD017109 (http://proteomecentral.proteomexchange.org/cgi/GetDataset?ID=PXD017109). Skyline files have been deposited to PanoramaWeb (https://panoramaweb.org/cGAS_PTM.url) and associated with the ProteomeXchange identifier PXD017133 (http://proteomecentral.proteomexchange.org/cgi/GetDataset?ID=PXD017133). The data can be accessed by the reviewers using the following information: 1) For the DDA dataset, username: reviewer88142@ebi.ac.uk and password: Pz8Ekmob, and 2) For PRM dataset, email: panorama+cristea6@proteinms.net and password: kqhMex3C.

References

1. Thompson MR, Kaminski JJ, Kurt-Jones EA, & Fitzgerald KA (2011) Pattern recognition receptors and the innate immune response to viral infection. *Viruses* 3(6):920-940.
2. Chen Q, Sun L, & Chen ZJ (2016) Regulation and function of the cGAS-STING pathway of cytosolic DNA sensing. *Nature immunology* 17(10):1142-1149.
3. Tan X, Sun L, Chen J, & Chen ZJ (2018) Detection of Microbial Infections Through Innate Immune Sensing of Nucleic Acids. *Annual review of microbiology* 72:447-478.
4. Wu J*, et al.* (2013) Cyclic GMP-AMP is an endogenous second messenger in innate immune signaling by cytosolic DNA. *Science* 339(6121):826-830.
5. Sun L, Wu J, Du F, Chen X, & Chen ZJ (2013) Cyclic GMP-AMP synthase is a cytosolic DNA sensor that activates the type I interferon pathway. *Science* 339(6121):786-791.
6. Li XD*, et al.* (2013) Pivotal roles of cGAS-cGAMP signaling in antiviral defense and immune adjuvant effects. *Science* 341(6152):1390-1394.
7. Lio CW*, et al.* (2016) cGAS-STING Signaling Regulates Initial Innate Control of Cytomegalovirus Infection. *Journal of virology* 90(17):7789-7797.
8. Paijo J*, et al.* (2016) cGAS Senses Human Cytomegalovirus and Induces Type I Interferon Responses in Human Monocyte-Derived Cells. *PLoS pathogens* 12(4):e1005546.
9. Wu JJ*, et al.* (2015) Inhibition of cGAS DNA Sensing by a Herpesvirus Virion Protein. *Cell host & microbe* 18(3):333-344.
10. Gao D*, et al.* (2013) Cyclic GMP-AMP synthase is an innate immune sensor of HIV and other retroviruses. *Science* 341(6148):903-906.
11. Mackenzie KJ*, et al.* (2017) cGAS surveillance of micronuclei links genome instability to innate

immunity. *Nature* 548(7668):461-465.
12. Harding SM*, et al.* (2017) Mitotic progression following DNA damage enables pattern recognition within micronuclei. *Nature* 548(7668):466-470.
13. Diner EJ*, et al.* (2013) The innate immune DNA sensor cGAS produces a noncanonical cyclic dinucleotide that activates human STING. *Cell reports* 3(5):1355-1361.
14. Ablasser A*, et al.* (2013) cGAS produces a 2'-5'-linked cyclic dinucleotide second messenger that activates STING. *Nature* 498(7454):380-384.
15. Ishikawa H & Barber GN (2008) STING is an endoplasmic reticulum adaptor that facilitates innate immune signalling. *Nature* 455(7213):674-678.
16. Zhong B*, et al.* (2008) The adaptor protein MITA links virus-sensing receptors to IRF3 transcription factor activation. *Immunity* 29(4):538-550.
17. Ishikawa H, Ma Z, & Barber GN (2009) STING regulates intracellular DNA-mediated, type I interferon-dependent innate immunity. *Nature* 461(7265):788-792.
18. Fitzgerald KA*, et al.* (2003) IKKepsilon and TBK1 are essential components of the IRF3 signaling pathway. *Nature immunology* 4(5):491-496.
19. Sharma S*, et al.* (2003) Triggering the interferon antiviral response through an IKK-related pathway. *Science* 300(5622):1148-1151.
20. Yoh SM*, et al.* (2015) PQBP1 Is a Proximal Sensor of the cGAS-Dependent Innate Response to HIV-1. *Cell* 161(6):1293-1305.
21. Orzalli MH*, et al.* (2015) cGAS-mediated stabilization of IFI16 promotes innate signaling during herpes simplex virus infection. *Proceedings of the National Academy of Sciences of the United States of America* 112(14):E1773-1781.
22. Chen M*, et al.* (2016) TRIM14 Inhibits cGAS Degradation Mediated by Selective Autophagy Receptor p62 to Promote Innate Immune Responses. *Molecular cell* 64(1):105-119.
23. Morchikh M*, et al.* (2017) HEXIM1 and NEAT1 Long Non-coding RNA Form a Multi-subunit Complex that Regulates DNA-Mediated Innate Immune Response. *Molecular cell* 67(3):387-399 e385.
24. Seo GJ*, et al.* (2018) TRIM56-mediated monoubiquitination of cGAS for cytosolic DNA sensing. *Nature communications* 9(1):613.
25. Lian H*, et al.* (2018) ZCCHC3 is a co-sensor of cGAS for dsDNA recognition in innate immune response. *Nature communications* 9(1):3349.
26. Lahaye X*, et al.* (2018) NONO Detects the Nuclear HIV Capsid to Promote cGAS-Mediated Innate Immune Activation. *Cell* 175(2):488-501 e422.
27. Liang Q*, et al.* (2014) Crosstalk between the cGAS DNA sensor and Beclin-1 autophagy protein shapes innate antimicrobial immune responses. *Cell host & microbe* 15(2):228-238.
28. Seo GJ*, et al.* (2015) Akt Kinase-Mediated Checkpoint of cGAS DNA Sensing Pathway. *Cell reports* 13(2):440-449.
29. Xia P*, et al.* (2016) Glutamylation of the DNA sensor cGAS regulates its binding and synthase activity in antiviral immunity. *Nature immunology* 17(4):369-378.
30. Wu MZ*, et al.* (2017) miR-25/93 mediates hypoxia-induced immunosuppression by repressing cGAS. *Nature cell biology* 19(10):1286-1296.
31. Wang Y*, et al.* (2017) Inflammasome Activation Triggers Caspase-1-Mediated Cleavage of cGAS to Regulate Responses to DNA Virus Infection. *Immunity* 46(3):393-404.
32. Lum KK*, et al.* (2018) Interactome and Proteome Dynamics Uncover Immune Modulatory Associations of the Pathogen Sensing Factor cGAS. *Cell systems* 7(6):627-642 e626.

33. Ghosh A*, et al.* (2019) Oligoadenylate-Synthetase-Family Protein OASL Inhibits Activity of the DNA Sensor cGAS during DNA Virus Infection to Limit Interferon Production. *Immunity* 50(1):51-63 e55.
34. Zhang G*, et al.* (2016) Cytoplasmic isoforms of Kaposi sarcoma herpesvirus LANA recruit and antagonize the innate immune DNA sensor cGAS. *Proceedings of the National Academy of Sciences of the United States of America* 113(8):E1034-1043.
35. Aguirre S*, et al.* (2017) Dengue virus NS2B protein targets cGAS for degradation and prevents mitochondrial DNA sensing during infection. *Nature microbiology* 2:17037.
36. Zhang J*, et al.* (2018) Species-Specific Deamidation of cGAS by Herpes Simplex Virus UL37 Protein Facilitates Viral Replication. *Cell host & microbe* 24(2):234-248 e235.
37. Huang J*, et al.* (2018) Herpes Simplex Virus 1 Tegument Protein VP22 Abrogates cGAS/STING-Mediated Antiviral Innate Immunity. *Journal of virology* 92(15).
38. Huang ZF*, et al.* (2018) Human Cytomegalovirus Protein UL31 Inhibits DNA Sensing of cGAS to Mediate Immune Evasion. *Cell host & microbe* 24(1):69-80 e64.
39. Biolatti M*, et al.* (2018) Human Cytomegalovirus Tegument Protein pp65 (pUL83) Dampens Type I Interferon Production by Inactivating the DNA Sensor cGAS without Affecting STING. *Journal of virology* 92(6).
40. Liu H*, et al.* (2018) Nuclear cGAS suppresses DNA repair and promotes tumorigenesis. *Nature* 563(7729):131-136.
41. Hu MM*, et al.* (2016) Sumoylation Promotes the Stability of the DNA Sensor cGAS and the Adaptor STING to Regulate the Kinetics of Response to DNA Virus. *Immunity* 45(3):555-569.
42. Dai J*, et al.* (2019) Acetylation Blocks cGAS Activity and Inhibits Self-DNA-Induced Autoimmunity. *Cell* 176(6):1447-1460 e1414.
43. Diner BA, Lum KK, Toettcher JE, & Cristea IM (2016) Viral DNA Sensors IFI16 and Cyclic GMP-AMP Synthase Possess Distinct Functions in Regulating Viral Gene Expression, Immune Defenses, and Apoptotic Responses during Herpesvirus Infection. *mBio* 7(6).
44. Kulak NA, Pichler G, Paron I, Nagaraj N, & Mann M (2014) Minimal, encapsulated proteomic-sample processing applied to copy-number estimation in eukaryotic cells. *Nature methods* 11(3):319-324.
45. Olsen JV*, et al.* (2009) A dual pressure linear ion trap Orbitrap instrument with very high sequencing speed. *Molecular & cellular proteomics : MCP* 8(12):2759-2769.
46. Guise AJ, Greco TM, Zhang IY, Yu F, & Cristea IM (2012) Aurora B-dependent regulation of class IIa histone deacetylases by mitotic nuclear localization signal phosphorylation. *Molecular & cellular proteomics : MCP* 11(11):1220-1229.
47. Scheltema RA*, et al.* (2014) The Q Exactive HF, a Benchtop mass spectrometer with a pre-filter, high-performance quadrupole and an ultra-high-field Orbitrap analyzer. *Molecular & cellular proteomics : MCP* 13(12):3698-3708.
48. Murray LA, Sheng X, & Cristea IM (2018) Orchestration of protein acetylation as a toggle for cellular defense and virus replication. *Nature communications* 9(1):4967.
49. Taus T*, et al.* (2011) Universal and confident phosphorylation site localization using phosphoRS. *Journal of proteome research* 10(12):5354-5362.
50. Fenyo D & Beavis RC (2003) A method for assessing the statistical significance of mass spectrometry-based protein identifications using general scoring schemes. *Analytical chemistry* 75(4):768-774.
51. Searle B.C. ECJ, Head B. (2013) Improving Peptide and Protein Identification Rates Using a Novel Semi-Supervised Approach in Scaffold (Abstract (3141)). *ASMS 61st Conference on Mass Spectrometry;*

Minnesota, United States.

52. The M, MacCoss MJ, Noble WS, & Kall L (2016) Fast and Accurate Protein False Discovery Rates on Large-Scale Proteomics Data Sets with Percolator 3.0. *Journal of the American Society for Mass Spectrometry* 27(11):1719-1727.
53. Omasits U, Ahrens CH, Muller S, & Wollscheid B (2014) Protter: interactive protein feature visualization and integration with experimental proteomic data. *Bioinformatics* 30(6):884-886.
54. MacLean B*, et al.* (2010) Skyline: an open source document editor for creating and analyzing targeted proteomics experiments. *Bioinformatics* 26(7):966-968.
55. Zhang Y*, et al.* (2014) The DNA sensor, cyclic GMP-AMP synthase, is essential for induction of IFN-beta during Chlamydia trachomatis infection. *Journal of immunology* 193(5):2394-2404.
56. Yang H, Wang H, Ren J, Chen Q, & Chen ZJ (2017) cGAS is essential for cellular senescence. *Proceedings of the National Academy of Sciences of the United States of America* 114(23):E4612-E4620.
57. Volkman HE, Cambier S, Gray EE, & Stetson DB (2019) Tight nuclear tethering of cGAS is essential for preventing autoreactivity. *eLife* 8.
58. Zhao Y & Jensen ON (2009) Modification-specific proteomics: strategies for characterization of post-translational modifications using enrichment techniques. *Proteomics* 9(20):4632-4641.
59. Olsen JV & Mann M (2013) Status of large-scale analysis of post-translational modifications by mass spectrometry. *Molecular & cellular proteomics : MCP* 12(12):3444-3452.
60. Sjoelund V, Smelkinson M, & Nita-Lazar A (2014) Phosphoproteome profiling of the macrophage response to different toll-like receptor ligands identifies differences in global phosphorylation dynamics. *Journal of proteome research* 13(11):5185-5197.
61. Thygesen C, Boll I, Finsen B, Modzel M, & Larsen MR (2018) Characterizing disease-associated changes in post-translational modifications by mass spectrometry. *Expert review of proteomics* 15(3):245-258.
62. Greco TM, Yu F, Guise AJ, & Cristea IM (2011) Nuclear import of histone deacetylase 5 by requisite nuclear localization signal phosphorylation. *Molecular & cellular proteomics : MCP* 10(2):M110 004317.
63. Miteva YV & Cristea IM (2014) A proteomic perspective of Sirtuin 6 (SIRT6) phosphorylation and interactions and their dependence on its catalytic activity. *Molecular & cellular proteomics : MCP* 13(1):168-183.
64. Unterholzner L*, et al.* (2010) IFI16 is an innate immune sensor for intracellular DNA. *Nature immunology* 11(11):997-1004.
65. Zhou W*, et al.* (2018) Structure of the Human cGAS-DNA Complex Reveals Enhanced Control of Immune Surveillance. *Cell* 174(2):300-311 e311.
66. Gao P*, et al.* (2013) Cyclic [G(2',5')pA(3',5')p] is the metazoan second messenger produced by DNA-activated cyclic GMP-AMP synthase. *Cell* 153(5):1094-1107.
67. Krissinel E & Henrick K (2007) Inference of macromolecular assemblies from crystalline state. *Journal of molecular biology* 372(3):774-797.
68. Ordureau A*, et al.* (2015) Defining roles of PARKIN and ubiquitin phosphorylation by PINK1 in mitochondrial quality control using a ubiquitin replacement strategy. *Proceedings of the National Academy of Sciences of the United States of America* 112(21):6637-6642.
69. Meyer JG*, et al.* (2016) Quantification of Lysine Acetylation and Succinylation Stoichiometry in Proteins Using Mass Spectrometric Data-Independent Acquisitions (SWATH). *Journal of the American Society for Mass Spectrometry* 27(11):1758-1771.

70. Morales Betanzos C, Federspiel JD, Palubinsky AM, McLaughlin B, & Liebler DC (2016) Dynamic Phosphorylation of Apoptosis Signal Regulating Kinase 1 (ASK1) in Response to Oxidative and Electrophilic Stress. *Chemical research in toxicology* 29(12):2175-2183.
71. Mankan AK*, et al.* (2014) Cytosolic RNA:DNA hybrids activate the cGAS-STING axis. *The EMBO journal* 33(24):2937-2946.
72. Gui X*, et al.* (2019) Autophagy induction via STING trafficking is a primordial function of the cGAS pathway. *Nature* 567(7747):262-266.
73. Li T & Chen ZJ (2018) The cGAS-cGAMP-STING pathway connects DNA damage to inflammation, senescence, and cancer. *The Journal of experimental medicine* 215(5):1287-1299.
74. Kwon J & Bakhoum SF (2020) The Cytosolic DNA-Sensing cGAS-STING Pathway in Cancer. *Cancer discovery* 10(1):26-39.
75. Sidoli S, Bhanu NV, Karch KR, Wang X, & Garcia BA (2016) Complete Workflow for Analysis of Histone Post-translational Modifications Using Bottom-up Mass Spectrometry: From Histone Extraction to Data Analysis. *Journal of visualized experiments : JoVE* (111).
76. Tsai CF*, et al.* (2015) Large-scale determination of absolute phosphorylation stoichiometries in human cells by motif-targeting quantitative proteomics. *Nature communications* 6:6622.
77. Zhou T, Chung YH, Chen J, & Chen Y (2016) Site-Specific Identification of Lysine Acetylation Stoichiometries in Mammalian Cells. *Journal of proteome research* 15(3):1103-1113.
78. Hansen BK*, et al.* (2019) Analysis of human acetylation stoichiometry defines mechanistic constraints on protein regulation. *Nature communications* 10(1):1055.
79. Chattopadhyay S*, et al.* (2010) Viral apoptosis is induced by IRF-3-mediated activation of Bax. *The EMBO journal* 29(10):1762-1773.
80. Sze A*, et al.* (2013) Host restriction factor SAMHD1 limits human T cell leukemia virus type 1 infection of monocytes via STING-mediated apoptosis. *Cell host & microbe* 14(4):422-434.
81. Petrasek J*, et al.* (2013) STING-IRF3 pathway links endoplasmic reticulum stress with hepatocyte apoptosis in early alcoholic liver disease. *Proceedings of the National Academy of Sciences of the United States of America* 110(41):16544-16549.
82. Zierhut C*, et al.* (2019) The Cytoplasmic DNA Sensor cGAS Promotes Mitotic Cell Death. *Cell* 178(2):302-315 e323.
83. Orzalli MH & Kagan JC (2017) Apoptosis and Necroptosis as Host Defense Strategies to Prevent Viral Infection. *Trends in cell biology* 27(11):800-809.
84. Perez-Riverol Y*, et al.* (2019) The PRIDE database and related tools and resources in 2019: improving support for quantification data. *Nucleic acids research* 47(D1):D442-D450.

Figures and Figure Legends

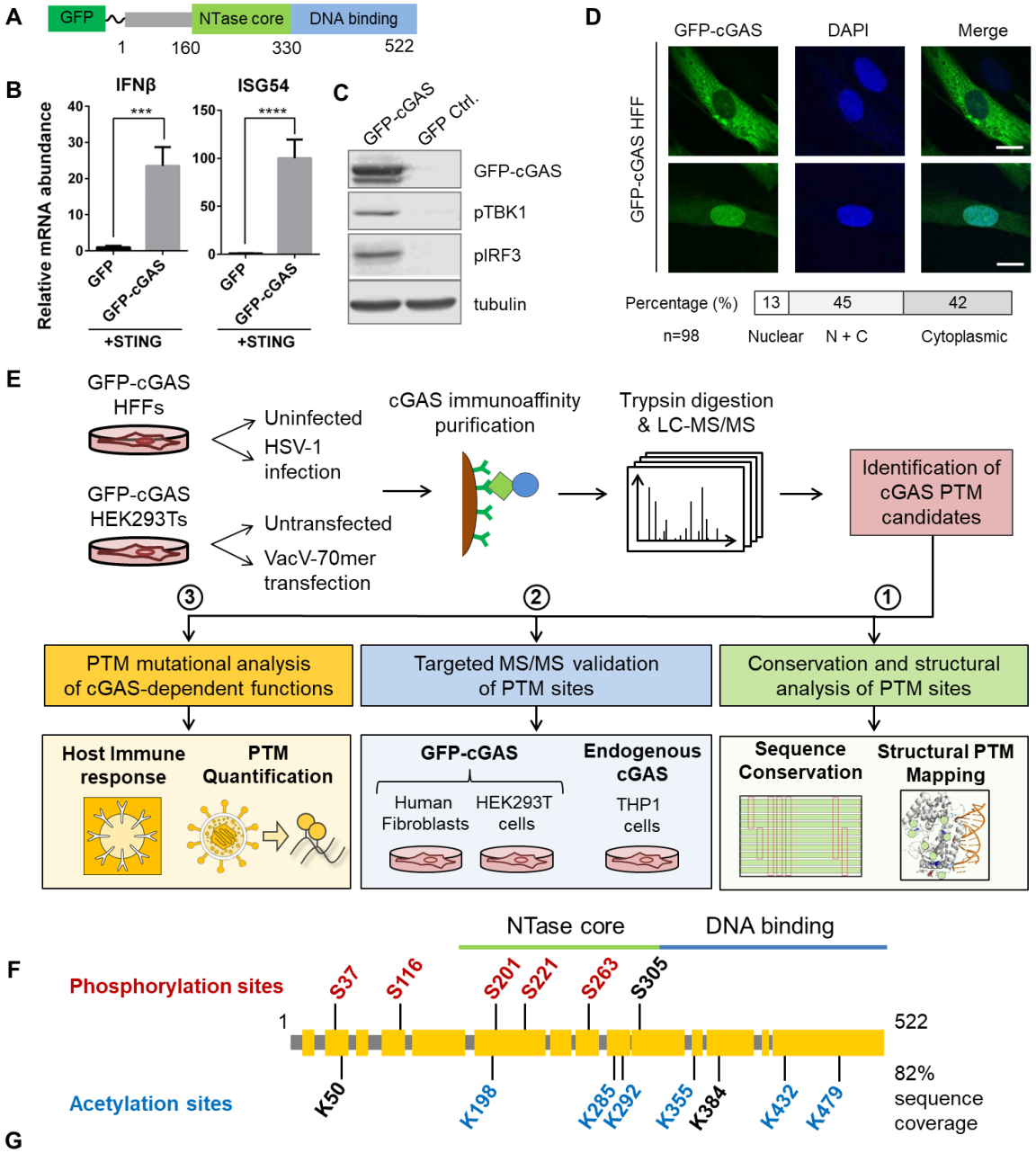

G

Site	Phosphorylated peptide	ptmRS
S37	GAPMDPTE**S**PAAPEAALPK	99.98
S116	AQDTQPSDATSAPGAEGLEPPAAREPAL**S**R	100
S201	CD**S**AFRGVGLLNTGSYYEHVK	100
S221	I**S**APNEFDVMFK	100
S263	ENPL**S**QFLEGEILSASK	100
S305	GG**S**PAVTLLISEK	100

Site	Acetylated peptide	ptmRS
K50	AG**K**FGPAR	100
K198	L**K**CDSAFR	100
K285	II**K**EEINDIKDTDVIMK	100
K292	EEINDI**K**DTDVIMK	100
K355	L**K**PFYLVPK	100
K384	LSFSHIE**K**EILNNHGK	100
K432	HLD**K**FSSYHVK	100
K479	TE**K**LENYFIPEFNLFSSNLIDK	100

Figure 1 Identification of cGAS phosphorylation and acetylation sites using IP-MS. (A) Diagram of N-terminal tagged GFP-cGAS. B) The GFP-cGAS construct is functional,

inducing cytokine expression in STING-HEK293T cells. IFN-β and ISG54 expressions were measured by qPCR experiments. Unpaired t test, ***: $P < 0.001$, ****: $P < 0.0001$ (mean ± SEM, N = 4). (C) The GFP-cGAS construct induces immune signaling, as shown by western blotting of phosphorylated IRF3 (pIRF3). (D) Primary human fibroblasts (HFFs) stably expressing GFP-cGAS. GFP-cGAS localizes to the cytoplasm and nucleus. Scale bar: 10μm. (E) Workflow for investigating cGAS PTMs. Using lentiviral transduction system, doxycycline-inducible GFP-cGAS human fibroblasts (HFFs) and GFP-cGAS STING HEK293T cells were constructed. PTMs were assessed following GFP-cGAS IP from uninfected and HSV-1 infected HFFs (multiplicity of infection of 5, 6 hpi), as well as from HEK293T cells with or without VacV70mer DNA transfection (6 hpt). The cGAS phosphorylations and acetylations identified from the IP-MS analyses were then validated by targeted MS/MS (PRM) in several cell systems and on endogenous cGAS. (F) Identified cGAS phosphorylation and acetylation sites. Previously unreported modifications are shown in red (phosphorylations) and blue (acetylations) and known modifications are in black. The cGAS sequence that was covered in the DDA analysis (82%) is shown in yellow. (see Fig. S4 for detailed sequence coverage). (G) Tryptic cGAS PTM peptides and their corresponding modified site (underlined) and localization score (ptmRS).

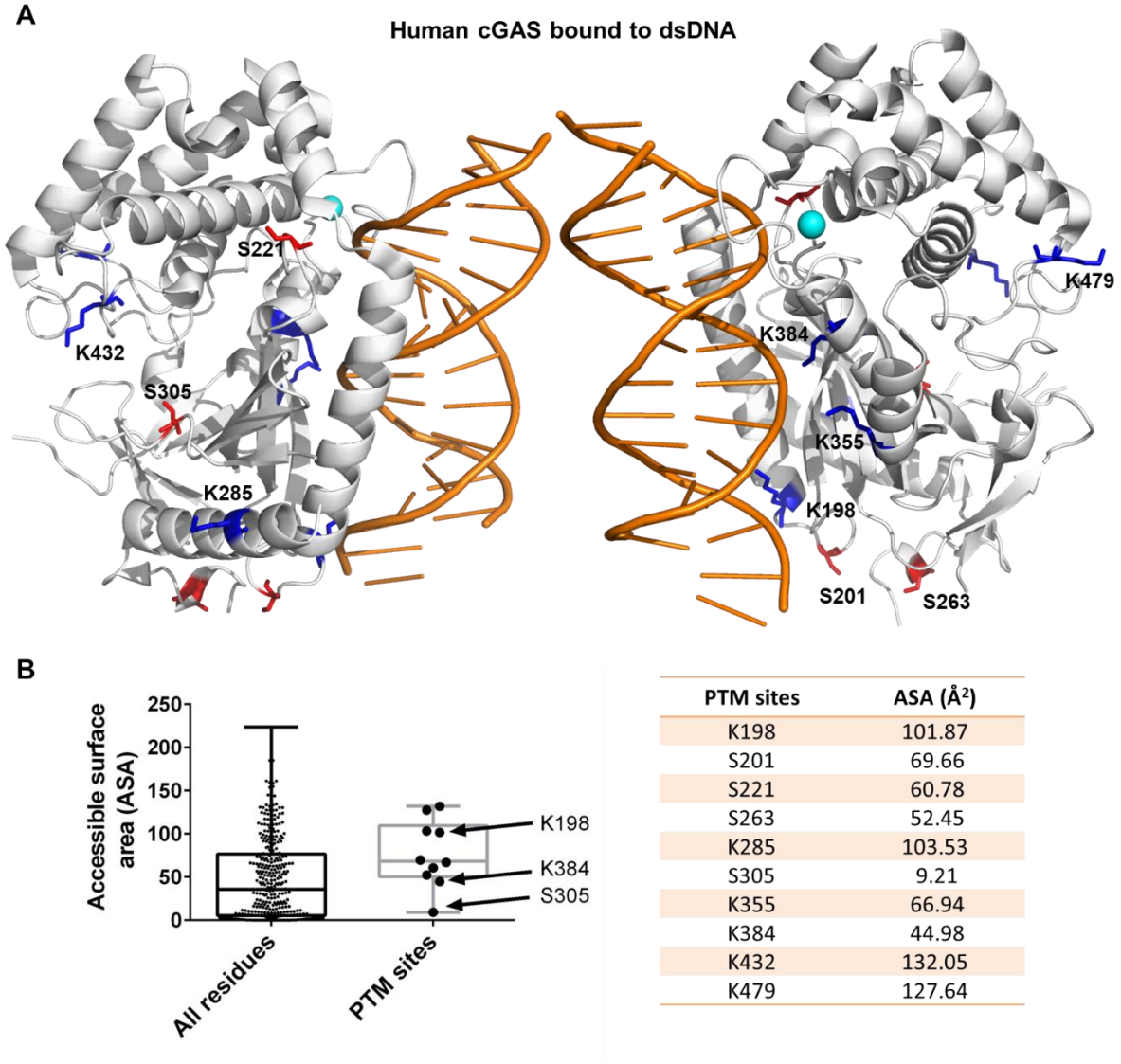

PTM sites	ASA (Å²)
K198	101.87
S201	69.66
S221	60.78
S263	52.45
K285	103.53
S305	9.21
K355	66.94
K384	44.98
K432	132.05
K479	127.64

Figure 2. Localization of the identified acetylation and phosphorylation sites within the human cGAS crystal structure. (A) The structure of human cGAS 161-521 with Zn^{2+} and bound dsDNA, adapted from Zhou W et al. *Cell* (2018). PDB: 6ct9. The phosphorylation sites on human cGAS sequence are labeled in red, and acetylation sites are in blue. (B) Accessible surface area (ASA) plotted for all residues versus modified sites. ASA values were calculated from the human cGAS structure (A) using PDBePISA.

		Species	common name	S37	S116	S201	S221	S263	S305	K50	K198	K285	K292	K355	K384	K432	K479
mammals	primates	Homo sapiens	human	S	S	S	S	S	S	K	K	K	K	K	K	K	K
		Pan troglodytes	chimpanzee	S	S	S	S	S	S	K	K	K	K	K	K	K	K
		Gorilla gorilla	gorilla	S	S	S	S	S	S	K	K	K	K	K	K	K	R
		Pongo abelii	Sumatran orangutan	S	S	S	S	S	S	K	Q	K	K	K	K	K	Q
		Macaca mulatta	rhesus monkey	S	S	P	S	S	S	K	K	K	K	K	K	K	Q
		Piliocolobus tephrosceles	Ugandan red colobus	S	S	S	S	S	S	K	K	K	K	K	K	K	K
		Chlorocebus aethiops	African green monkey	S	S	S	S	S	S	K	K	K	K	K	K	K	K
		Papio anubis	olive baboon	S	S	S	S	S	S	K	K	K	K	K	K	K	K
		Saguinus fuscicollis	brown-mantled tamarin	S	S	S	S	R	S	K	K	K	Q	K	K	K	K
		Aotus nancymaae	Ma's night monkey	S	S	S	S	R	S	K	Q	K	Q	K	K	K	K
	rodents	Mus musculus	mouse	T	S	S	S	S	S	S	Q	K	K	E	K	A	K
		Rattus norvegicus	rat	T	L	S	S	S	S	S	Q	K	K	E	S	A	K
		Heterocephalus glaber	naked mole-rat	S	G	G	S	S	S	K	Q	K		H	K	K	E
		Octodon degus	degu	F	D	S	S	D	S	L	K	K	T	E	K	K	E
	even-toed ungulates	Sus scrofa	wild boar		G	S	S	E	S	R	Q	K	E	Q	K	K	Q
		Neophocaena asiaeorientalis	finless porpoise	S	G	S	S	G	S	R	Q	K	E	Q	K	K	Q
	carnivores	Felis catus	domestic cat	S	G	S	S	S	S	K	K	K	E	Q	K	K	H
		Enhydra lutris kenyoni	sea otter	P	G	S	S	I	S	M	Q	K	Q	Q	K	K	Q
		Neomonachus schauinslandi	Hawaiian monk seal	P	G	S	S	S	S	K	Q	K	Q	Q	K	K	Q
	bats	Pteropus vampyrus	large flying fox	S	G	S	S	R	S	R	Q	K	K	E	K	E	H
	odd-toed ungulates	Equus caballus	horse	C	S	S	S	S	S	S	Q	K	E	Q	K	K	R
birds		Cyanistes caeruleus	Eurasian blue tit					S	S			K	K	K	K	K	Q
		Numida meleagris	helmeted guineafowl			G	S	N	S		R	K	K	K	K	K	Q
bony fishes		Danio rerio	zebra fish	Q	N	T	C	D	C	D	K	K	T	Q	K	S	Q
		Oryzias melastigma	marine medaka	Q	E	Q	S	K	C	K	K	T	K	K	K	E	K
turtles		Terrapene mexicana triunguis	three toed box turtle	H	S	S	S	D	S	R	R	K	T	K	K	K	Y
bivalves		Mizuhopecten yessoensis	Japanese scallop			Q	E	Y	G		R	D	R	C	R	I	H
insects	flies	Drosophila busckii	fruit fly			P	C		G		S	S	Q	R	R	A	K
	beetles	Anoplophora glabripennis	Asian long-horned beetle			T	G		G		K	T	E	Y	R	K	K
	ants	Pseudomyrmex gracilis	Mexican twig ant			P	G	K	G		K	G	N	R	K	N	K
corals		Stylophora pistillata	smooth cauliflower coral			S	C		G		E	S	Q	C	K	L	E

Figure 3. Evolutionary conservation analysis for cGAS modification sites. Amino acid sequences for cGAS from different species were acquired from NCBI and aligned by Clustal Omega. The phylogenetic tree of species' names was based on NCBI taxonomy. Conserved serine residues were colored in red and conserved lysine residues were colored in blue.

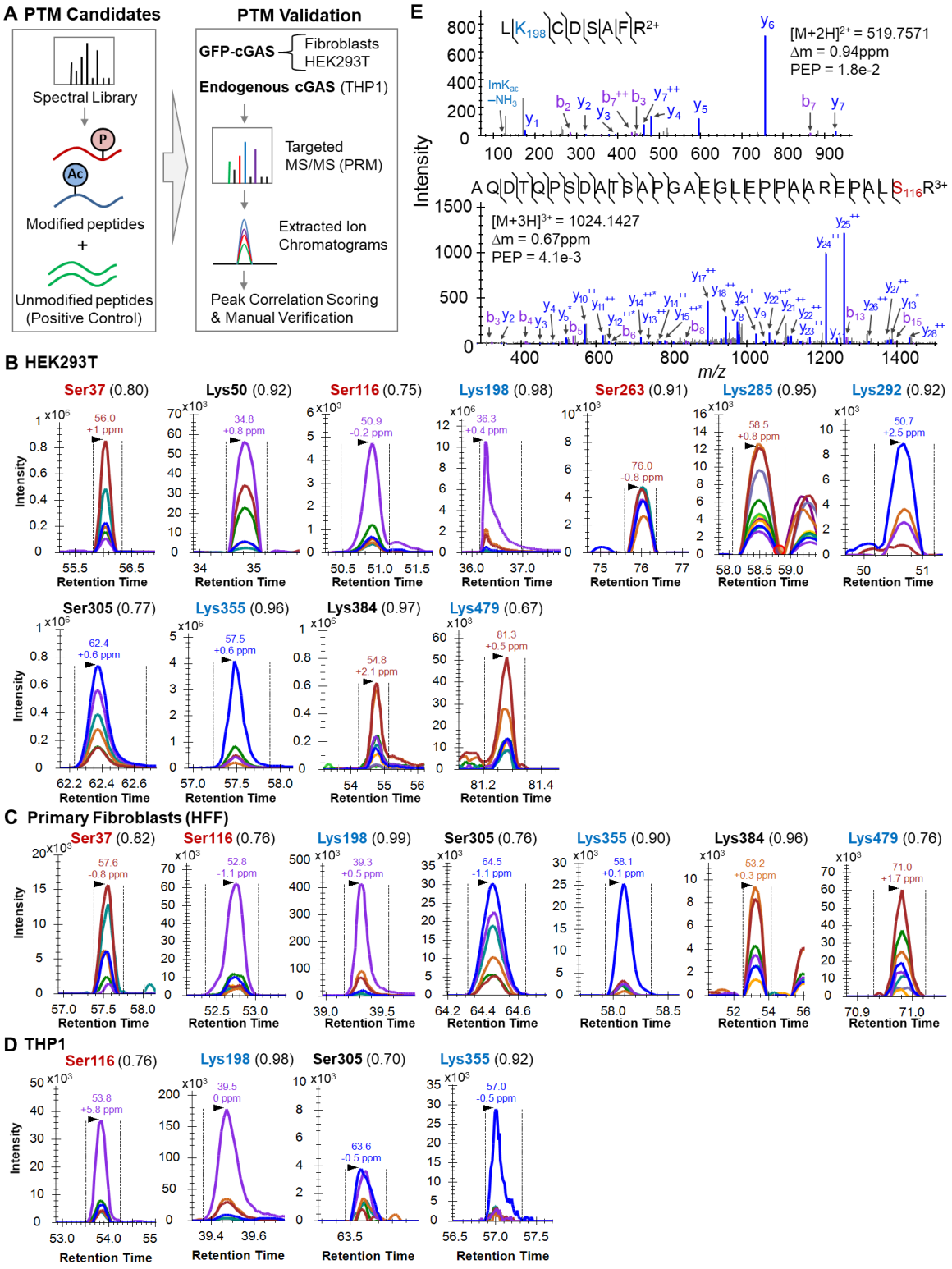

Figure 4. Validation of cGAS PTMs by targeted mass spectrometry analysis. (A) Workflow of parallel reaction monitoring (PRM) analysis of cGAS modifications. A spectral library was designed for modified and unmodified cGAS peptides. (B-D) Representative extracted fragment ion chromatograms (n ≥ 4 co-eluting fragments) are shown for cGAS

modified tryptic peptides that were validated in ≥ 2 biological replicates in at least one cell type for (B) HEK293T, (C) HFF, and D) THP1 cells. The peak correlation to the library spectra (dotp) is indicated in parentheses. (E) Representative MS/MS spectra from the library that support cGAS acetylation at Lys198 (HCD) and phosphorylation at Ser116 (CID). For simplicity, only selected y and b ions (including neutral losses, *) are labeled in the spectra. Manual verification of fragment ion assignments for y and b ions are indicated along the peptide sequence. The measured precursor *m/z*, mass error (Δm), and Percolator match probability (PEP) are indicated.

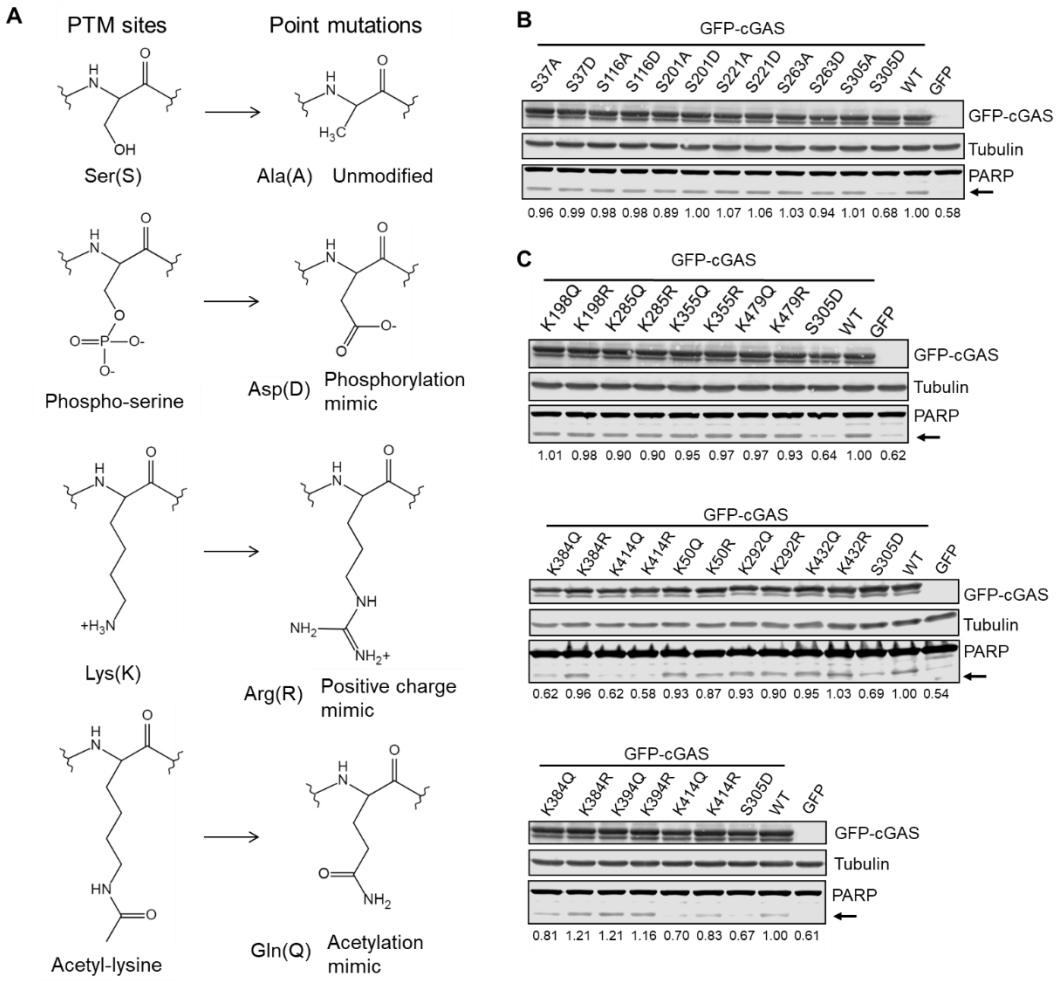

Figure 5. cGAS PTM mutants affect cGAS-dependent apoptosis induction. (A) Ser sites found as phosphorylated were mutated into Ala or Asp to represent an unmodified state or a modified mimic, respectively. Acetylated Lys sites were mutated into Gln or Arg as an acetylation mimic or a positive charge mimic. (B & C) The impact of cGAS mutations on apoptosis induction was assessed at 22 h post transfection by quantifying PARP cleavage with western blotting. Relative quantification of PARP cleavage was calculated by densitometry as the ratio of cleaved PARP (arrow) to total PARP signal, normalized to WT (displayed values). The S305D mutation was used as a positive control for inhibition of cGAS-dependent PARP cleavage.

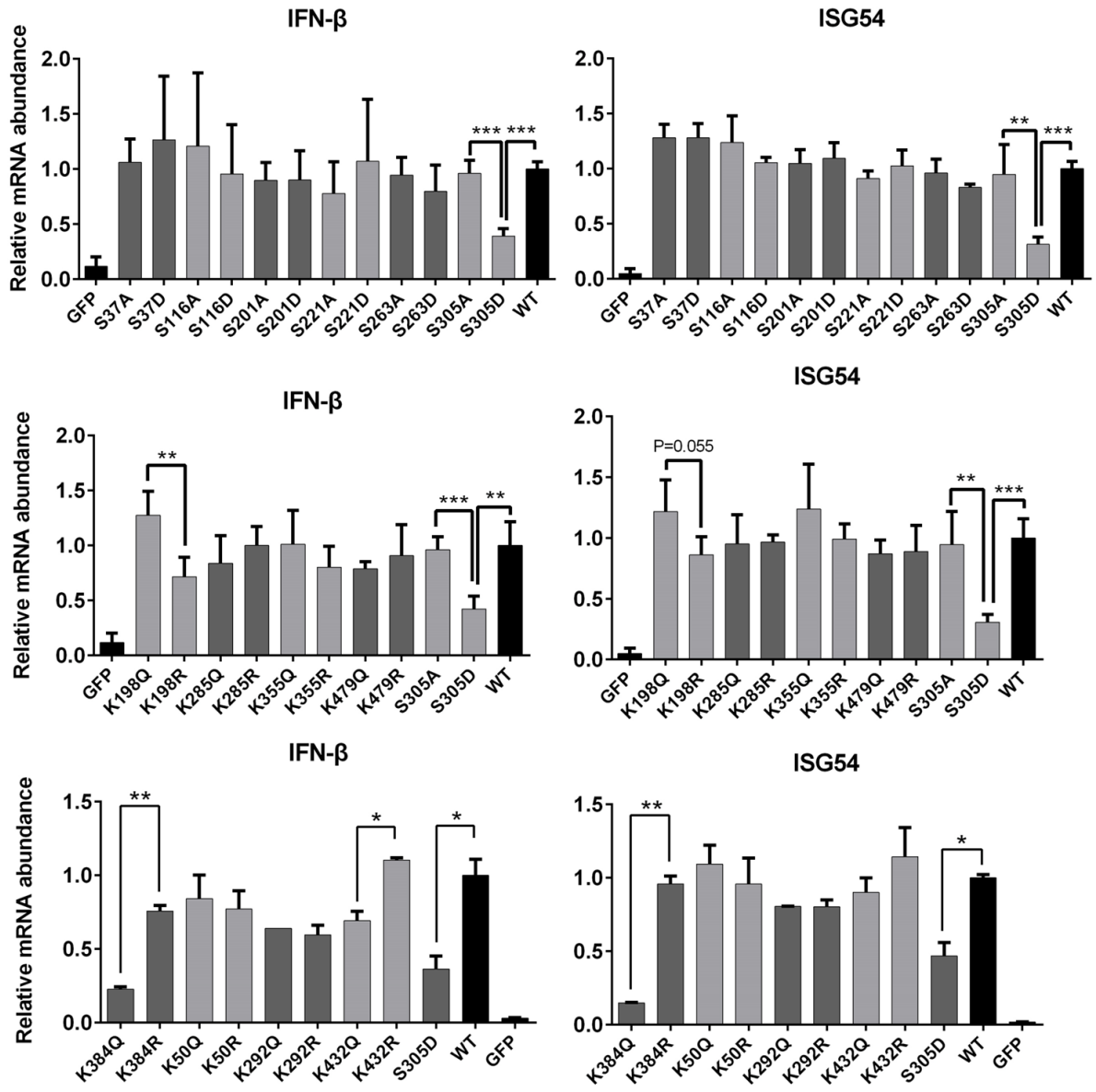

Figure 6. cGAS PTM mutants modulate cGAS-dependent immune signaling. IFN-β (*left*) and ISG54 (*right*) expression levels were measured by qPCR in HEK293T cells co-transfected with STING and either GFP alone, GFP-cGAS (WT), or GFP-cGAS mutants at 16 h post transfection. The mRNA abundance is normalized to WT sample. Significance testing was performed for pairwise A vs. D and Q vs. R cGAS mutants, except for S305D, which was also compared with WT as a positive control. Only pairs that reached significance are labeled. Unpaired t test, *, $p < 0.05$; **, $p < 0.01$; ***, $p < 0.001$ (mean ± SEM, N = 4).

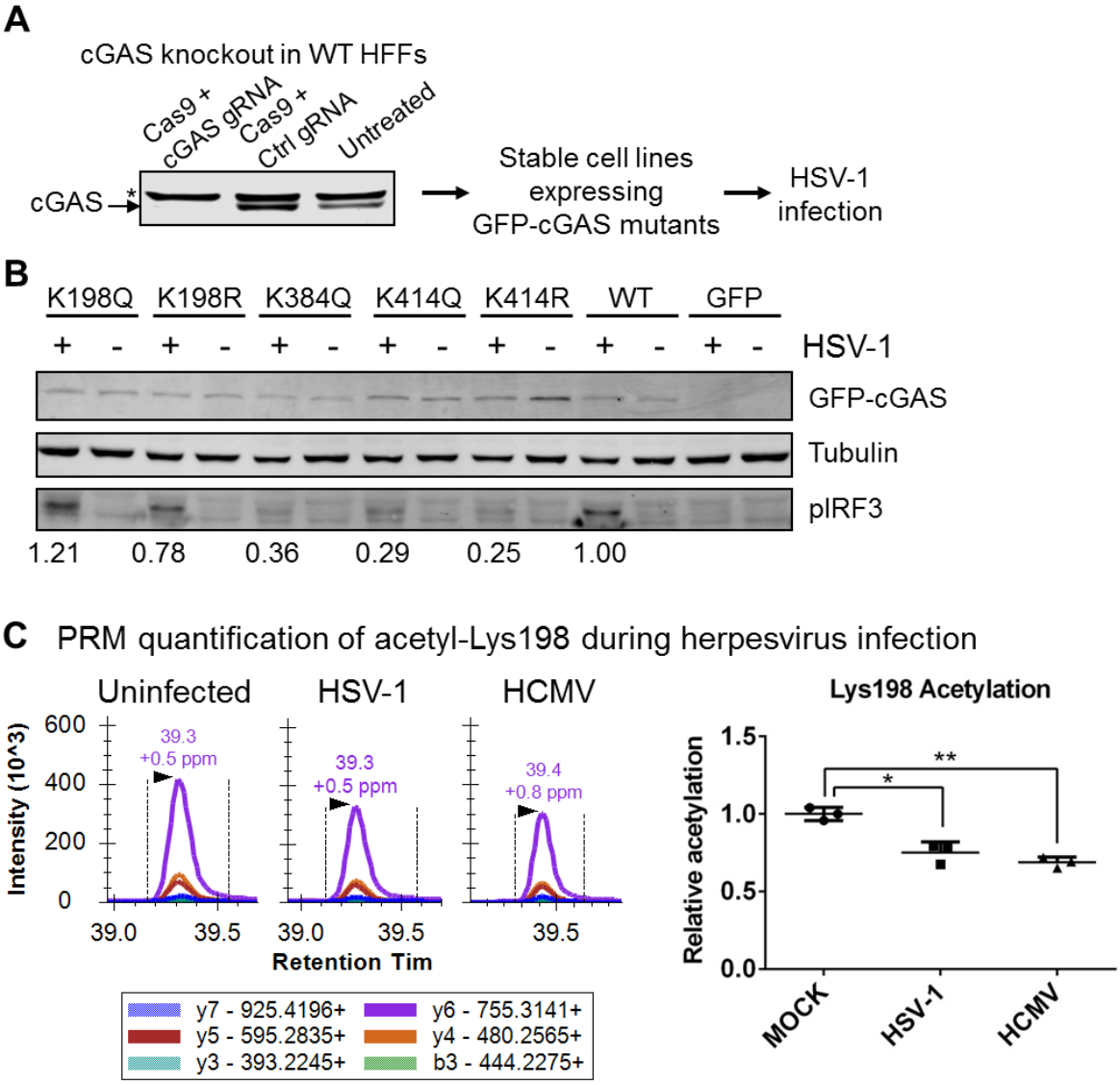

Figure 7. cGAS PTM mutants differentially impact immune signaling during herpesvirus infection. (A) Workflow for generating HFF lines expressing cGAS mutants in CRISPR-mediated cGAS knockout background. Western blot shows knockout efficiency of cGAS compared to controls (untreated and Cas9 + Ctrl gRNA). *, non-specific band. (B) The effect of cGAS mutations on the levels of phosphorylated IRF3 (pIRF3) in the absence (-) and presence (+) of HSV-1 infection at 6 hours post infection (hpi). Relative quantification of pIRF3 was calculated by densitometry as the ratio of pIRF3 to mutant GFP-cGAS during HSV-1 infection. (C) Representative raw extracted fragment ion chromatograms acquired by PRM analysis of the acetylated-Lys198 peptide from uninfected, HSV-1, and HCMV infected HFF cells at 6 hpi. The summed peak areas of the top three fragment ions (y4 – y6) were used to calculate virus-induced changes in Lys198 acetylation. Acetylation levels were normalized

by total cGAS abundance and expressed relative to uninfected controls. Unpaired t test, *, $p < 0.05$; **, $p < 0.01$ (mean ± SEM, N = 3).